Heliyon 10 (2024) e35368

Contents lists available at ScienceDirect

Heliyon

journal homepage: www.cell.com/heliyon

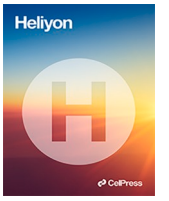

Research article

Pan-cancer investigation of RFX family and associated genes identifies RFX8 as a therapeutic target in leukemia

Zelong Cui [a], Yue Fu [a,b], Minran Zhou [a], Huimin Feng [a], Lu Zhang [a], Sai Ma [a,**], Chunyan Chen [a,*]

[a] Department of Hematology, Qilu Hospital, Cheeloo College of Medicine, Shandong University, Jinan, China
[b] Department of Physiology and Pathophysiology, School of Basic Medical Science, Cheeloo College of Medicine, Shandong University, Jinan, Shandong, China

ARTICLE INFO

Keywords:
Pan-cancer
Regulatory factor X
Regulatory factor X associated
AML
Chelerythrine

ABSTRACT

Background: Several transcription factors and co-factors are encoded by the RFX (Regulatory Factor X) family (RFX1-8) and associated genes (RFXAP and RFXANK). Increasing evidence suggests that the RFX family and associated genes are involved in the development and progression of cancer. However, no prior research has focused on a multi-omic analysis of these genes to evaluate their role in tumor progression.

Methods: Using combined TCGA and GTEx pan-cancer data, we investigated the expression patterns and survival profiles of these ten genes. We then focused on RFX8 to analyze its clinicopathological and therapeutic features. Finally, we conducted experimental validation of RFX8 function in acute myeloid leukemia (AML).

Results: RFX5 and RFXANK showed higher expression levels, while RFX6 showed lower expression levels in most types of cancer, with RFX8 being the most upregulated in LAML. RFX2 and RFXAP demonstrated prognostic significance in eight types of cancer, and RFX8 showed significance in six types of cancer. The expression of these ten genes exhibited specific characteristics in immune subtypes, tumor microenvironment, and stemness. The expression of RFX8 was correlated with various tumor stages, microsatellite instability (MSI), tumor mutation burden (TMB), immune cell infiltration, and immune-checkpoint expression. Additionally, RFX8 was found to regulate tumorigenesis and sensitivity to chelerythrine in AML.

Conclusions: Our work delineated the landscape of the RFX family and associated genes in the pan-cancer context and the specific role of RFX8 in AML. These findings might offer cues for further investigations of these genes in cancer biology.

1. Background

A group of transcription factors (TFs) encoded by the RFX (Regulatory Factor binding to the X-box, or Regulatory Factor X) gene family share a distinctive DNA-binding domain. Unlike other TFs with a helix-turn-helix domain, RFX TFs recognize DNA with their β-hairpin (wing) in the winged-helix binding domain [1]. Eight RFX TFs regulate genes involved in numerous developmental and

* Corresponding author.
** Corresponding author.
E-mail addresses: masai09563@qiluhospital.com (S. Ma), chency@sdu.edu.cn (C. Chen).

https://doi.org/10.1016/j.heliyon.2024.e35368
Received 30 January 2024; Received in revised form 24 July 2024; Accepted 26 July 2024
Available online 28 July 2024

cellular processes in humans [2]. During the development of embryos, vision formation, olfaction, and spermatogenesis, RFX1, RFX2, RFX3, and RFX4 modulate ciliogenesis [3,4]. RFX6 regulates pancreatic islet cell development [5]. Recently, RFX7 has been found to regulate the homeostasis of NK cells through metabolism [6]. The existence of the RFX8 protein has recently been identified, but little is known about its function. RFX5 regulates the transcription of major histocompatibility complex (MHC) genes. Notably, two important cofactors, RFXAP and RFXANK, form a heterometric complex with RFX5 to regulate the transcription of MHC II. These genes collectively play essential roles in the development of the immune system [7].

The majority of cancers, if not all, exhibit TF dysregulation, which contributes to tumor aggression. The abnormal expression of TFs in cancer cells prevents normal differentiation and cell death while regulating endogenous signaling to drive proliferation and migration. Additionally, TF dysregulation may result in drug resistance and immune evasion [8]. It is not surprising that RFX TFs also function in these processes. RFX1 is abnormally expressed in several types of cancer and interferes with various cellular processes, making it an ideal target for cancer therapy [9]. Transcriptome analysis has associated RFX2 with ovarian and non-small cell lung cancers [10,11]. Breast cancer and glioma tumors are thought to be driven by RFX3 [12,13]. RFX4 could serve as a marker for early glioma detection due to its differentially expressed isoforms in healthy individuals and glioma patients [14]. RFX5 acts as an activator in tumorigenesis, whereas RFXAP is a suppressor [15,16]. RFX6 regulates tumor invasiveness and T cell immune response in liver cancer [17]. RFX7 is generally downregulated in lymphoid neoplasms [18], especially Burkitt lymphoma. RFX7 inhibits AKT and mTOR signaling through cooperation with p53, demonstrating a tumor suppressor role [19]. Although previous analyses suggested that RFX8 has clinical significance in several types of cancer, only a recent report described its function as a DDX24 transcriptional activator that stimulates liver cancer [20,21]. Previous studies have often focused on a few specific genes and lacked comprehensive analysis across cancer types. Besides, more knowledge about the function of RFX8 is needed.

In this paper, we employed bioinformatics methods to analyze the relationship between ten RFX family and associated genes (referred to as RFX-related genes) and 33 types of cancer. We measured differential expression, survival status, stemness, and immune microenvironment scores for all genes. We then focused on RFX8 by analyzing its correlation with cancer stages, immune cell fractions, and expression of immune-related molecules. Finally, we validated the function of RFX8 in AML cell lines. Our work demonstrated the landscape of RFX-related genes across cancers and the specific role of RFX8 in AML.

Table 1
Samples used for analysis.

Abbreviation Name	Full Name	Number of tumor samples	Number of normal samples
ACC	Adrenocortical carcinoma	79	128
BLCA	Bladder Urothelial Carcinoma	411	28
BRCA	Breast invasive carcinoma	1104	292
CESC	Cervical squamous cell carcinoma and endocervical adenocarcinoma	306	13
CHOL	Cholangiocarcinoma	36	9
COAD	Colon adenocarcinoma	471	349
DLBC	Lymphoid Neoplasm Diffuse Large B-cell Lymphoma	48	337
ESCA	Esophageal carcinoma	162	668
GBM	Glioblastoma multiforme	168	1157
HNSC	Head and Neck squamous cell carcinoma	502	44
KICH	Kidney Chromophobe	65	53
KIRC	Kidney renal clear cell carcinoma	535	100
KIRP	Kidney renal papillary cell carcinoma	289	60
LAML	Acute Myeloid Leukemia	173	337
LGG	Brain Lower Grade Glioma	529	1152
LIHC	Liver hepatocellular carcinoma	374	160
LUAD	Lung adenocarcinoma	526	347
LUSC	Lung squamous cell carcinoma	501	338
MESO	Mesothelioma	86	–
OV	Ovarian serous cystadenocarcinoma	379	88
PAAD	Pancreatic adenocarcinoma	178	171
PCPG	Pheochromocytoma and Paraganglioma	183	3
PRAD	Prostate adenocarcinoma	499	152
READ	Rectum adenocarcinoma	167	10
SARC	Sarcoma	263	2
SKCM	Skin Cutaneous Melanoma	471	558
STAD	Stomach adenocarcinoma	375	211
TGCT	Testicular Germ Cell Tumors	156	165
THCA	Thyroid carcinoma	510	338
THYM	Thymoma	119	339
UCEC	Uterine Corpus Endometrial Carcinoma	548	23
UCS	Uterine Carcinosarcoma	56	78
UVM	Uveal Melanoma	80	–

2. Materials and Methods

2.1. Public data acquisition

Multimodal data of 33 types of cancer were retrieved from the combined cohort "TCGA TARGET GTEx" in UCSC XENA. We selected TCGA and GTEx samples with complete gene expression, clinical information, and mutation data to facilitate our analysis. Table 1 lists the samples we used.

2.2. Differential expression Gene (DEG) analysis

The analysis between tumor and normal samples was conducted in the pan-cancer cohort using the limma package in R. DEG comparison was made using the Wilcoxon test. Then, the correlation matrix for each pair of genes was conducted with the Pearson correlation test. The pheatmap package was used to draw heatmaps, and the corrplot package was used to draw the correlation plots. Cancer types with three or fewer normal samples were excluded from DEG analysis.

2.3. Survival and cancer stage analysis

The survival analysis of RFX-related genes in various cancer types was conducted using both Kaplan-Meier (KM) and univariate COX regression analyses. For KM analysis, the median expression of genes was used as the cutoff. AJCC stage data for non-neurological and non-hematological tumors were used for cancer stage comparison. Four stages were used to compare gene expression, and these were measured using the Wilcoxon test.

2.4. Immune and microenvironment-related analysis

The immune subtype data were retrieved from previous research. Six subtypes were identified in TCGA non-hematological tumor samples, named "wound healing" (C1),"IFN-γ dominant" (C2), "inflammatory" (C3), "lymphocyte depleted" (C4), "immunologically quiet" (C5), and "TGF-β dominant" (C6) [22]. Six subtypes were compared per gene between samples using the Kruskal-Wallis test. From solid cancer expression data, the ESTIMATE algorithm was used to calculate stromal and immune cell scores and their aggregation, known as ESTIMATE scores. These scores reflect relative levels of infiltrating stromal and immune cells, and tumor purity [23]. CIBERSORT was used to estimate the immune cell fraction based on expression data [24]. Several previous studies were used to compile the immune checkpoint gene list summary [25,26]. The DEG between subtypes was compared using the Wilcoxon test. For ESTIMATE and CIBERSORT analyses, the correlation of gene expression with these scores was done using the Pearson correlation test. The corrplot package was used to depict the correlation plots.

2.5. Stemness score, microsatellite instability (MSI), and tumor mutation burden (TMB)

The one-class logistic regression (OCLR) algorithm was used to establish stemness indices per sample based on transcriptomic and DNA methylation data [27]. MSI, a hypermutation pattern in genomic microsatellites with predictive and prognostic significance for certain cancers, was retrieved from previous research [28]. To determine TMB, the number of somatic variants in the TCGA whole exome sequencing (WES) data was divided by the target region's size, with the estimated exome size being 38 Mb [29]. The Pearson correlation test was used to analyze the correlation between these three scores and the expression of RFX and RFX-related genes. The corrplot package was used to draw the correlation map of the stemness score, while the radar map of MSI and TMB was depicted using the FMSB package.

2.6. Drug sensitivity prediction

CellMiner (Version 2022.1) was used to extract drug activity and gene expression data across the NCI-60 cell panel [30]. Drug sensitivity is represented as normalized IC50, where a higher value indicates increased resistance. The Pearson correlation test was used to determine the relationship between gene expression and drug activity, which was then visualized using the corrplot package.

2.7. Patients and sample preparation

Bone marrow aspirate was collected from ten patients with de novo AML and ten patients with iron-deficiency anemia (IDA). IDA samples served as normal controls [31]. Mononuclear cells were isolated and stored at −80 °C. These procedures received informed consent from patients and were approved by the ethics committee of Qilu Hospital, Shandong University (Ethical approval number: KYLL-2020(KS)-535).

2.8. Cell culture, construction of Lentiviral-transfected cells, and Compound

The U937 cell line was provided by the American Type Culture Collection (ATCC), and the THP-1 cell line was purchased from Shanghai Zhong Qiao Xin Zhou Biotechnology Co., Ltd. Both cell lines were cultured in RPMI 1640 medium with 10 % heat-inactivated

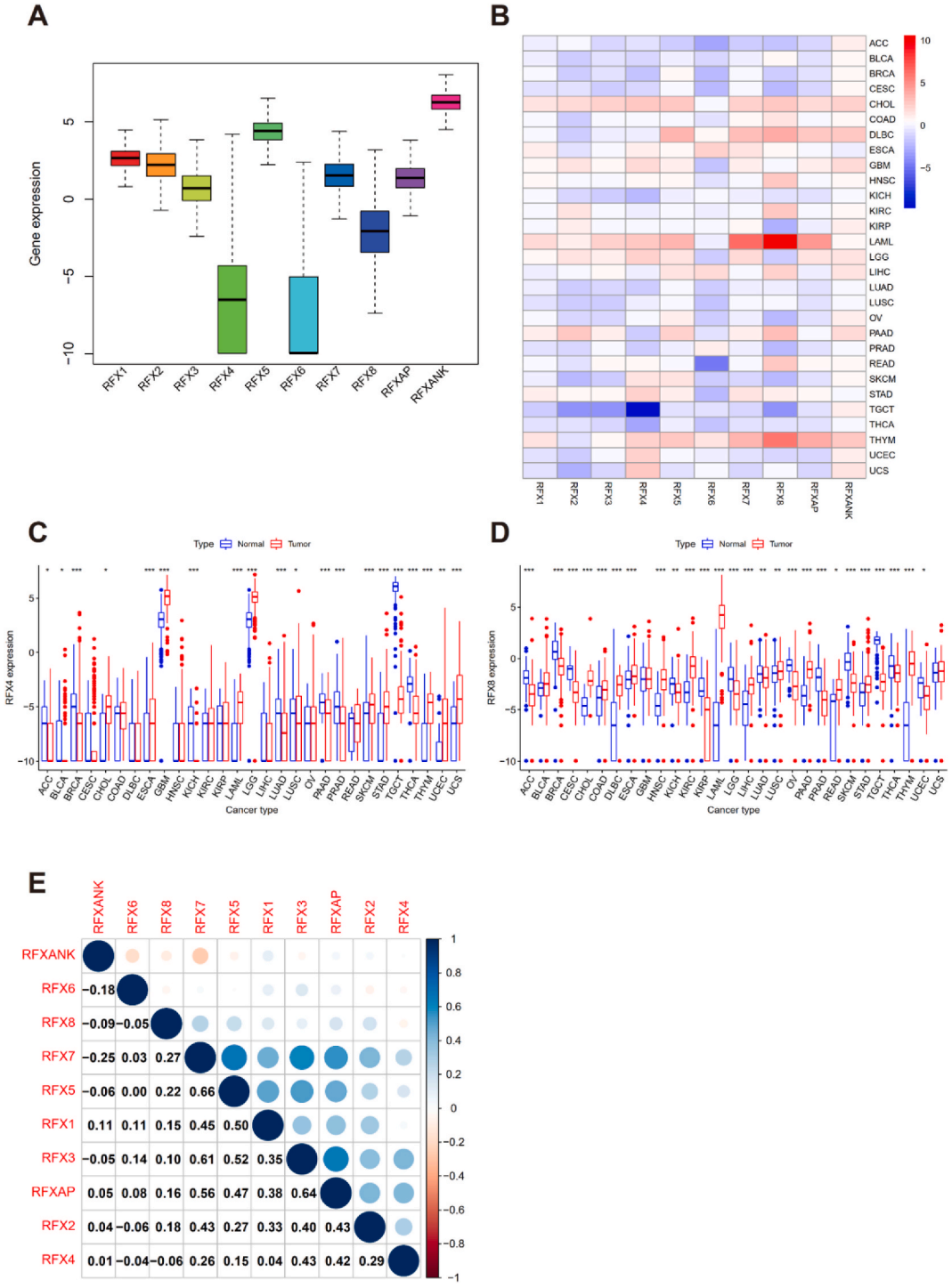

Fig. 1. Differential Expression and Co-Expression Analysis of 10 RFX Genes (A) Gene expression in pan-cancer. **(B)** The heatmap shows expression levels of Rfx 8 genes among 33 cancer types; the color transition represents changes in log 2 Fold Change (log FC) value. **(C and D)** The differential expression of RFX 4 and RFX 8 between tumor and normal samples in 31 cancer types (***p < 0.001; **p < 0.01; *p < 0.05). (E) Co-expression heatmap demonstrates the co-expression relationships of RFX genes. The correlation coefficients are shown in separate boxes. (For interpretation of the references to color in this figure legend, the reader is referred to the Web version of this article.)

fetal bovine serum (FBS; Gibco, Carlsbad, CA, USA) and maintained in an incubator at 37 °C and 5 % CO_2 without antibiotics.

The RFX8 shRNA lentivirus, provided by Shanghai GeneChem Co., Ltd., targeted the sequence 5′-GCTGATGTCATTGCCTGACGT-3′, with a control sequence of 5′-TTCTCCGAACGTGTCACGT-3'. On day 1, the lentivirus was transfected with a multiplicity of infection (MOI) of 120. Twelve hours post-transfection, the medium was changed. On day 3, cells were further selected with puromycin (2 μg/ml) for about three days. Knockdown efficacy was measured by changes in RNA and protein expression levels. Chelerythrine (HY–N2359) was purchased from MCE (Shanghai, China) and dissolved in DMSO.

2.9. RNA Extraction and real-time Quantitative PCR

Total RNA was extracted using the Trizol reagent (Invitrogen, Carlsbad, CA, United States) according to the manufacturer's instructions. The extracted RNA was reverse transcribed using the Evo M-MLV RT Kit with gDNA Clean for qPCR (Accurate Biology, Hunan, China). The resulting cDNAs were mixed with SYBR Green (Accurate Biology, Hunan, China) for real-time PCR analysis. The following is a list of the primers used in real-time PCR tests.

Gene	Forward Primer	Reverse Primer
RFX8	5′-CTTCCTGGTGGACACTGCCATG-3′	5′-GGGTTATGAGGGCTTCTTGTCC-3′
Actin	5′-AGTTGCGTTACACCCTTTCTTG-3′	5′-CACCTTCACCGTTCCAGTTTT-3′

2.10. Western Blot

Total protein was extracted with protease inhibitors in RIPA buffer (Beyotime, Shanghai, China), then quantified on ice. Proteins were separated by SDS-PAGE gels before being transferred to PVDF membranes (Millipore, Bedford, MA). After blocking and washing, the membranes were incubated overnight at 4 °C with specific primary antibodies against RFX8 (1:400, rabbit, Atlas Antibodies, HPA059745) and Beta Actin (1:5000, rabbit, Proteintech, 66009-1-Ig). This was followed by a 1-h incubation with horseradish peroxidase-labeled goat-anti-rabbit/mouse IgG (1:4000, Jackson ImmunoResearch). Immunoblots were probed with an ECL detection reagent from Millipore following standard procedures.

2.11. Cell proliferation assay: CCK-8 and 5-ethynyl-2′-Deoxyuridine (EdU) assay

To detect the proliferation rates of U937 and THP-1 cells, a 5-ethynyl-2′-deoxyuridine (EdU) assay was used. Cells were incubated with EdU for 2 h, smeared on a glass slide, and fixed with 4 % paraformaldehyde for 30 min. The Cell-Light EdU Apollo 488 In Vitro Kit (RioBio, China) was used to stain the cells according to the manufacturer's instructions. The slides were examined with fluorescence microscopy, and the proportion of EdU-positive cells in total cells was calculated and compared. Three replicates were performed per group, and significance was quantified using a *t*-test.

For the CCK-8 assay, cells were seeded in triplicate in 96-well plates at 10,000 to 15,000 cells per well to examine the effects of chelerythrine and RFX8 knockdown on cell viability. Cell proliferation and viability were assessed using the Cell Counting Kit-8 (CCK-8; APExBIO, Houston, USA) following the manufacturer's instructions. Three replicates were performed per group, and comparisons were made using Student's t-test. Cells used in the EdU assay and CCK-8 assay were stably knocked down or treated with chelerythrine for 48 h.

2.12. IC50 Calculation

Cells were treated with increasing concentrations of chelerythrine for 48 h. Relative viability was assessed using the CCK-8 assay with three replicates. The IC50 was calculated by correlating log-transformed concentration and relative viability values.

2.13. Statistical significance

We regarded $p < 0.05$ as significant for the Wilcoxon test, Kruskal-Wallis test, Pearson correlation, and Student's t-test. Asterisks indicate significance levels: * for $p < 0.05$, ** for $p < 0.01$, and *** for $p < 0.001$.

3. Results

3.1. Expression profile of 10 RFX and associated genes

The workflow is shown in the Graphical Abstract. Fig. 1A depicts the expression of 10 RFX-related genes. Using the Wilcoxon test, the 10 RFX-related genes were found to be differentially expressed in tumors and matched normal samples for 29 different types of cancer (Fig. 1B–Table S1). There is a noticeable variance in gene expression among tumors. Gene expression varies significantly between tumors. Upregulation of these genes is predominant in CHOL, DLBC, LAML, and THYM. Genes are generally downregulated in ACC, BLCA, BRCA, CESC, and TGCT. The expression pattern of each gene across cancers is generally contradictory (Fig. S1). RFXANK

and RFX5 rank first and second with upregulation in 28 (96 %) and 20 (68 %) types of cancer, respectively. Moreover, RFX6 is downregulated in 20 (68 %) types of cancer. RFX4 from TGCT has the lowest fold change of approximately −9.7, while RFX8 from LAML has the highest at about 10.5 (Fig. 1C and D). Regarding gene co-expression status, most genes share positive co-expression, with the strongest relationships observed between RFX5-RFX7, RFX3-RFXAP, and RFX3-RFX7 (Fig. 1E).

3.2. Survival analysis of 10 RFX and associated genes

Univariate COX regression was conducted for ten genes across 33 cancer types (Fig. 2A–H represents RFX1-8, Fig. 2I for RFXAP and Fig. 2J for RFXANK). The distribution of significant hazard ratios (HR) is generally sparse. As shown below, HRs of RFX2 and RFXAP

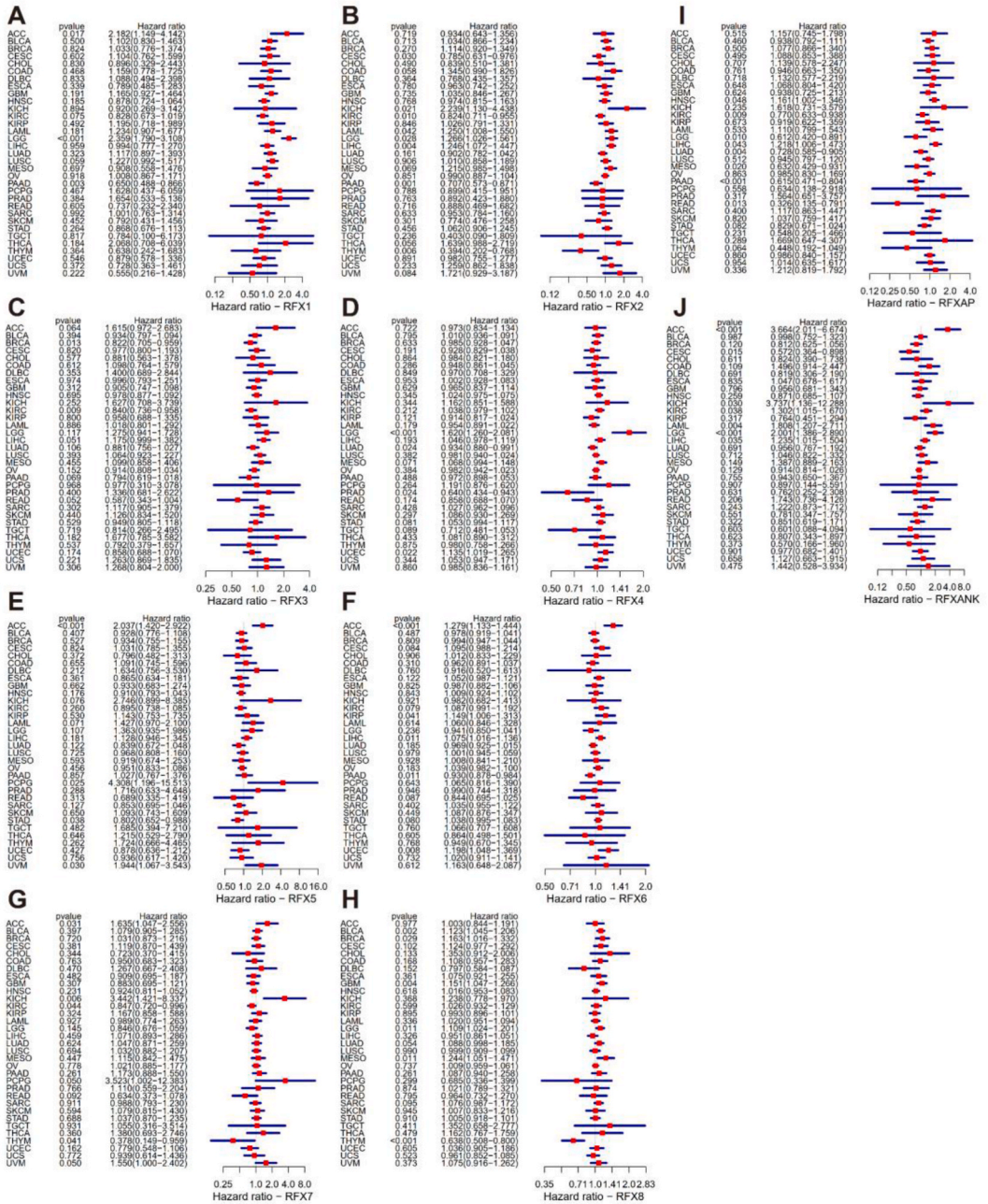

Fig. 2. Cox proportional model analysis of RFX genes in 33 cancer types. **(A–J)** Cox proportional hazard analyses of RFXs in TCGA cancers. Those with $p < 0.05$ are shown in red text. (For interpretation of the references to color in this figure legend, the reader is referred to the Web version of this article.)

are significant in eight types of cancer, while HRs of RFX8 are significant in six types of cancer. HRs of RFXANK and RFX3 are significant in only two types. Notably, in the LGG background, six genes are associated with prognosis. The predictions made by COX analysis were confirmed by additional Kaplan-Meier (KM) analysis (Fig. S2). In accordance with the COX results, high expression indicates a poor prognosis for RFX1 in COAD, RFX5 in ACC, RFX6 in UCEC, and RFX7 in ACC. Low expression indicates a poor prognosis for RFX2 in CESC, RFX3 in BRCA, RFX4 in PRAD, RFX8 in THYM, and RFXAP in PAAD.

3.3. Immune subtype analysis

We compared the differential expression levels of the 10 RFX-related genes across six immune subtypes in 33 TCGA cancer types (Fig. 3A). The expression of these ten genes shows significant differences among the six immune subtypes ($p < 0.001$). The expression levels of the 10 genes were then analyzed in three cancer types (Fig. 3B–D). In BRCA, LIHC, and STAD, the expression of these genes shows significant variance among the six immune subtypes. All three types of cancer showed significant differences in the expression of RFX1, RFX2, RFX6, RFX7, and RFXANK across subtypes ($p < 0.05$). Notably, RFX1 was expressed higher in C3 of these three cancers, and RFX8 was significantly higher ($p < 0.001$) in the C6 immune subtypes of BRCA and STAD. Similarly, the C1 and C2 immune subtypes had the highest RFXANK expression levels in LIHC and STAD ($p < 0.001$), suggesting that RFXANK may serve as an indicator of immune subtypes.

3.4. Tumor microenvironment and stemness analysis

In non-hematological tumors, we calculated the ESTIMATE score, stromal score, and immune score to examine their connections to RFX and the expression of its associated genes (Fig. 4A–C). Most cancers show a positive correlation ($p < 0.001$) with RFX5 and RFX8 expression. We then analyzed the relationships between gene expression and calculated epigenetic (DNAss) and transcriptomic (RNAss) stemness scores (Fig. 4D and E, Table S2). The highest positive correlations in DNAss were RFX2 in OV (coefficients = 0.5), RFX3 in GBM (coefficients = 0.435), RFX5 in PCPG (coefficients = 0.44), and RFX8 in SARC (coefficients = 0.432). The highest positive correlations in RNAss were RFX2 in THYM (coefficients = 0.586), RFX5 in PCPG (coefficients = 0.510), RFX8 in LAML (coefficients = 0.503), and RFXANK in THYM (coefficients = 0.530) (all $p < 0.001$).

3.5. Clinical features of RFX8 in pan-cancer

The function of RFX8 in various cancer types is poorly understood. Consequently, our further analysis and investigation focused on this gene. Under univariate Cox regression, RFX8 expression positively correlates with prognosis in BLCA, BRCA, GBM, LGG, and MESO but negatively correlates with prognosis in THYM (Fig. 2F). Under KM analysis, RFX8 expression positively correlates with prognosis in BLCA, CHOL, GBM, KIRP, and LGG but negatively correlates with prognosis in PCPG (Figs. S3A–F). Cancer stage analysis showed diverse RFX8 expression across several representative types of cancer (Fig. 5A–I). In COAD, KIRP, and READ, expression in Stage IV is higher than in Stage I. In BLCA and CHOL, Stage IV expression is higher than in Stage II. However, in THCA, Stage IV expression is slightly lower than in Stage I. In LIHC, LUSC, and MESO, there is no significant variance in the expression of RFX8.

3.6. MSI, TMB, immune Cell proportion, and immune checkpoint genes correlation of RFX8 in pan-cancer

There is growing evidence suggesting that MSI and TMB values are predictive biomarkers for response to targeted therapy and immunotherapy [32,33]. Considering this, we analyzed RFX8 expression and MSI/TMB values (Fig. 6A and B). Our analysis shows that RFX8 expression positively correlates with TMB in LGG, LUAD, and SARC, while it negatively correlates with TMB in BRCA, THYM, and UCEC (all $p < 0.01$). Regarding MSI, RFX8 expression positively correlates with MSI in LUSC, SARC, STAD, and UCEC but negatively correlates with MSI in DLBC (all $p < 0.01$). These findings suggest that RFX8 can be used as a potential marker of MSI and TMB status.

The infiltration of specific immune cells in tumor tissue can affect immune response. $CD8^+$ T cells and M1 macrophages are regarded as anti-cancer, while Treg and M2 macrophages are pro-cancer. We observed the correlations of RFX8 expression with immune cell fractions (Fig. 6C). For macrophages, RFX8 expression positively correlates with the M2 cell ratio in several types of cancer, including BLCA, COAD, HNSC, SARC, TGCT, and THCA, while it positively correlates with the M1 cell ratio in ACC, KIRC, KIRP, LGG, and LUAD (all $p < 0.01$). Additionally, in ACC and LGG, RFX8 expression positively correlates with the $CD8^+$ T cell ratio ($p < 0.05$), which aligns with the RFX8-M1 cell correlation in these two types of cancer. To understand RFX8's role in immunotherapy, we examined the relationship between immune checkpoint gene expression and RFX8 expression in pan-cancer (Fig. 6D). There is a positive correlation between RFX8 and PD-L1 (CD274) in numerous cancer types, including ACC, BLCA, COAD, HNSC, KICH, KIRC, LGG, LIHC, LUAD, LUSC, OV, PAAD, PCPG, PRAD, SARC, SKCM, STAD, TGCT, UCEC, and UVM. Similarly, a positive correlation was observed between RFX8 and PD-1 (PDCD1) in some cancer types (HNSC, KICH, KIRC, LGG, LIHC, LUAD, PRAD, and THYM). Additionally, RFX8 expression is positively correlated with other markers, such as CD160, CD27, CD80, CD28, and CTLA-4, in more than five types of cancer. These results suggest that RFX8 can serve as a predictive marker for immune cell fraction and molecular immunotherapy across different tumors.

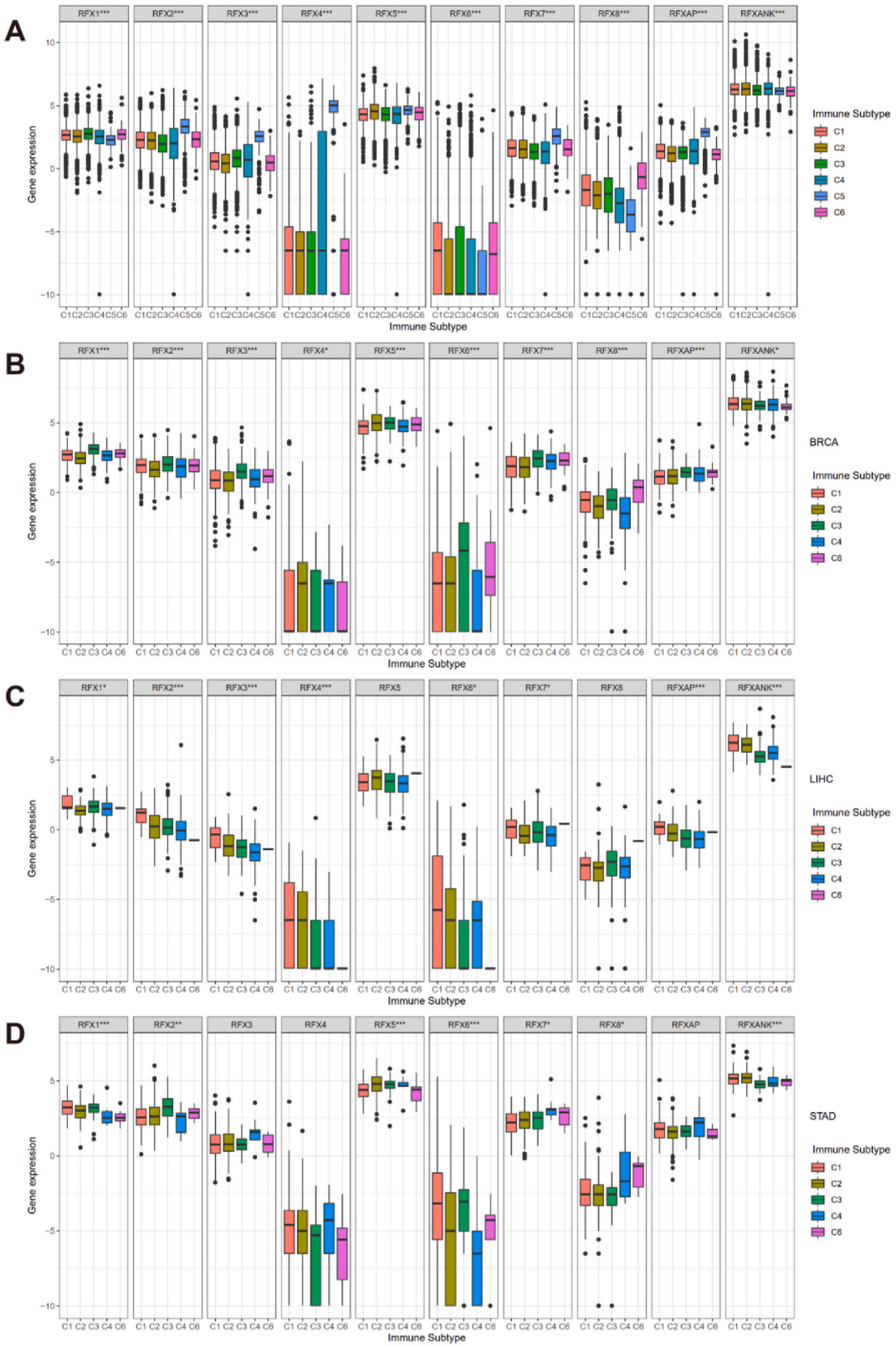

(caption on next page)

Fig. 3. Results of 10 RFX Gene Co-expression Analysis with Six Immune Subtypes **(A)** The differential expression of the RFX genes with different immune subtypes in all tumor types. **(B–D)** The correlation analysis between 10 RFX gene in BRCA, LIHC, and STAD and immune subtypes. (***:$p < 0.001$; **:$p < 0.01$; *: $p < 0.05$). **(D and E)** The two heatmaps show the correlation of expression level of 10 RFX genes and stemness indices (DNAss and RNAss) in 33 TCGA cancer types. (DNAss: DNA methylation-based stemness score; RNAss: RNA-based stemness score).

3.7. RFX8 knockdown inhibits AML Cell line proliferation

Acute myeloid leukemia (AML) is the most common leukemia among the adult population. The 5-year survival rate is around 30 %, and the refractory/relapse rate is around 40 %, making it one of the most challenging cancers to overcome. According to the results above, RFX8 expression shows a relatively high fold change (10.5) in LAML patients compared to healthy controls. The expression of RFX8 is associated with stemness indices in LAML cohorts (0.50 in RNAss and 0.25 in DNAss, all $p < 0.001$). Although RFX8 has no prognostic significance in LAML cohorts, in silico analysis indicates that RFX8 may regulate proliferation in AML as well as drug sensitivity. First, we validated RFX8 expression in our own samples, where de novo AML patients showed higher RFX8 expression than normal controls (Fig. 7A). We then used the AML cell lines U937 and THP-1 to create RFX8 knockdown cell lines. Knockdown efficiency was validated at mRNA and protein levels (Fig. 7B–C, Fig. S4). Following knockdown, cell proliferation was measured using the CCK-8 assay at 24h and the EdU assay at 72h. The CCK-8 assay showed significant viability loss in both cell lines (Fig. 7D). The EdU assay results were similar, with the knockdown effect on proliferation was evident in both U937 and THP-1 cell lines (Fig. 7E and F).

3.8. RFX8 enhances the sensitivity of AML cells to chelerythrine

Biomarkers are crucial for defining phenotypes and predicting therapy responses, integral to precision medicine [34]. Building on initial findings, we investigated whether RFX8 expression correlates with drug sensitivity. Using the pharmacogenomic database CellMiner, we found that higher RFX8 expression correlates with higher IC50 values for several standard chemotherapeutic agents in AML, including cytarabine, daunorubicin, arsenic trioxide, and etoposide (Fig. 8A, Table S3). Although the highest correlation was observed with nelarabine (NEL), combining RFX8 knockdown with NEL had no effect, even at doses up to 200 μM (Figs. S3G and S3H). Consequently, we focused on the second-highest correlated drug, chelerythrine (CHE).

CHE effectively kills AML cells, with an IC50 around 15 μM in U937 cells. RFX8 knockdown lowers the IC50 to approximately 5 μM (Fig. 8B). The EdU assay confirmed these findings, showing a similar pattern (Fig. 8C). These results suggest that RFX8 is a functional target for enhancing drug sensitivity and inhibiting tumor proliferation in AML.

4. Discussion

Advancements in detection technology in molecular biology have enabled the exploration of disease etiology at the molecular level. This has facilitated the deciphering of gene-disease relationships, contributing to an in-depth understanding and control of diseases. Previous studies have shown that RFX1 regulates tumor progression, drug resistance, and cancer metastasis [35–37]. RFX2 has been found to positively regulate PAF1 expression, maintaining stemness in spinal ependymoma [38]. RFX3, RFX4, and RFX5 are also reported to play roles in cancer progression or suppression. However, there has been no pan-cancer study on RFX-related genes until now. Through a data-driven analysis, we aimed to uncover the complex roles of RFX-related genes in pan-cancer and identify interesting features for individual genes and cancer types.

Firstly, we examined the expression and prognosis of RFX-related genes across various cancers. RFXANK and RFX5 were upregulated in most cancer types. Although reports on RFXANK in cancer are rare, RFX5 has been documented to be highly expressed in cancer samples and to affect cancer progression in liver, breast, and lung cancers [15,39,40]. Our analysis showed that RFXAP was downregulated and negatively correlated with prognosis in pancreatic adenocarcinoma (PAAD). Previous research has reported that higher RFXAP expression upregulates KDM4A, inducing H3K36 demethylation, leading to DNA damage and cell cycle arrest [16] Conversely, RFX6 was upregulated and positively correlated with prognosis in liver hepatocellular carcinoma (LIHC), supported by findings that the RFX6–PGAM1 axis promotes aerobic glycolysis and tumor progression in liver cancer [41].

We then investigated the characteristics of RFX-related genes in pan-cancer using bioinformatics analyses, including immune subtype, tumor microenvironment (TME), and stemness scores. Six immune subtypes were first calculated and interpreted from TCGA multi-omic data by Vésteinn et al. [22]. In our analysis, RFX4 expression was higher in C5 ("immunologically quiet"), mainly due to the enrichment of lower-grade glioma (LGG) and glioblastoma multiforme (GBM) samples in C5. C5 is associated with a better outcome due to fewer immune cell interactions [42]. The TME consists of non-tumor cells and matrix, and interactions between tumor cells and TME significantly impact tumor progression. The correlation between RFX-related gene expression and TME (ESTIMATE) and Stemness Scores suggests that these genes play a role in TME construction and the maintenance of cancer stem cells.

There have been some reports on the differential expression or genetic variance of RFX8 in various physiological or pathological contexts, including adipocyte differentiation [43], fatty liver [44], bladder cancer [45], and kidney cancer [46]. While the detailed structure of RFX8 transcripts was recently identified, its specific function remains unknown [2]. Our results showed that RFX8 expression is highly upregulated in acute myeloid leukemia (LAML). Cox regression and survival analyses revealed that RFX8 is a prognostic factor in BLCA, BRCA, GBM, LGG, MESO, and THYM. RFX8 has significance for prognosis in BLCA, CHOL, GBM, KIRP, LGG, and PCPG for KM analysis. The discrepancy between Cox and KM analyses may arise from the arbitrary cutoff for group division in KM plots. Additionally, RFX8 was upregulated in the C6 immune subtype, which is associated with an immunosuppressed TME, leading to

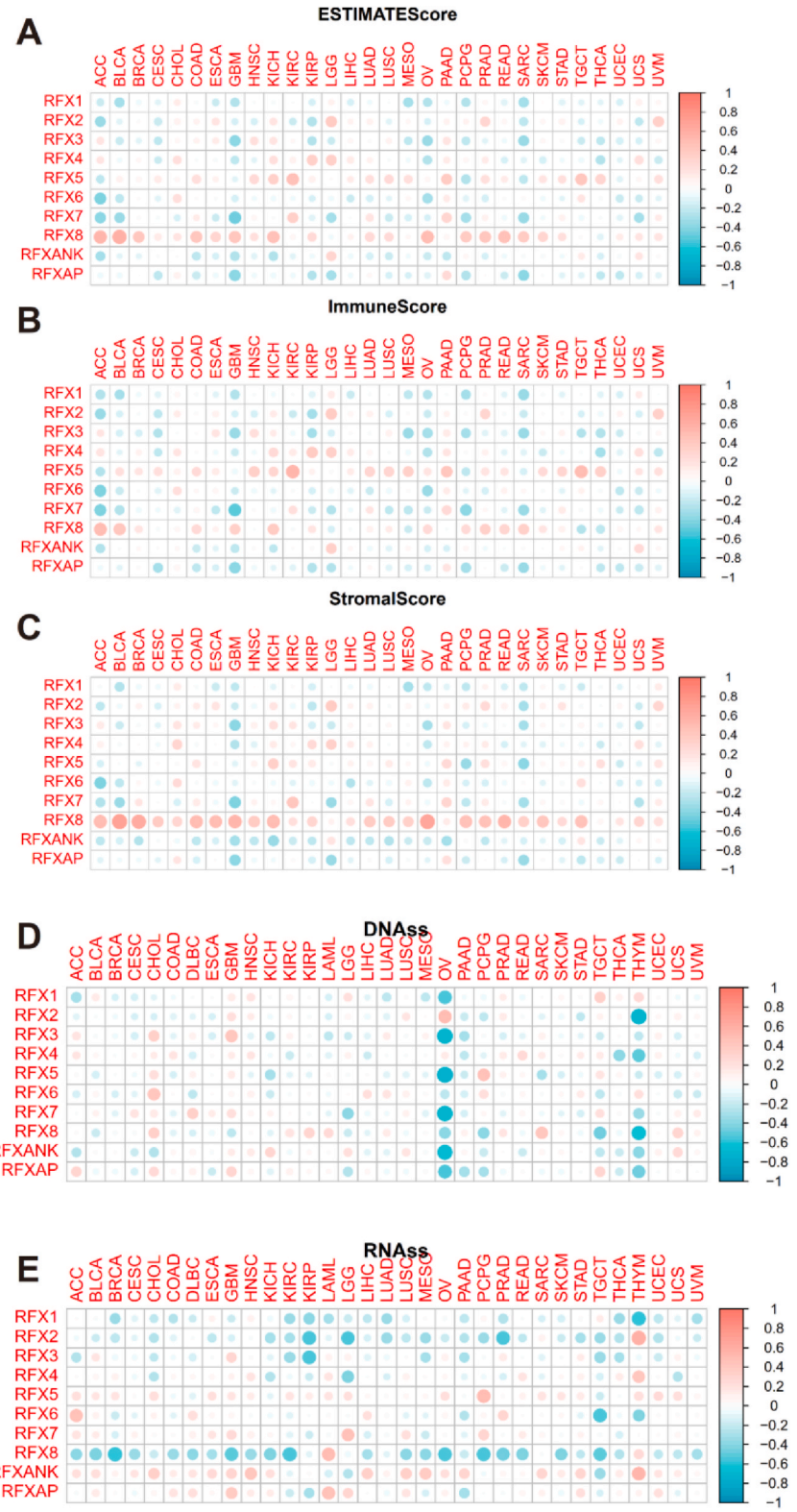

Fig. 4. Correlation Analysis of 10 RFX Genes with Tumor Stemness Score and Tumor Microenvironment Score **(A–C)** Correlation analysis of 10 RFX genes expression with ESTIMATE immune and stromal score in 30 cancer types. (Positive and negative correlations are indicated by red and blue dots, respectively). (For interpretation of the references to color in this figure legend, the reader is referred to the Web version of this article.)

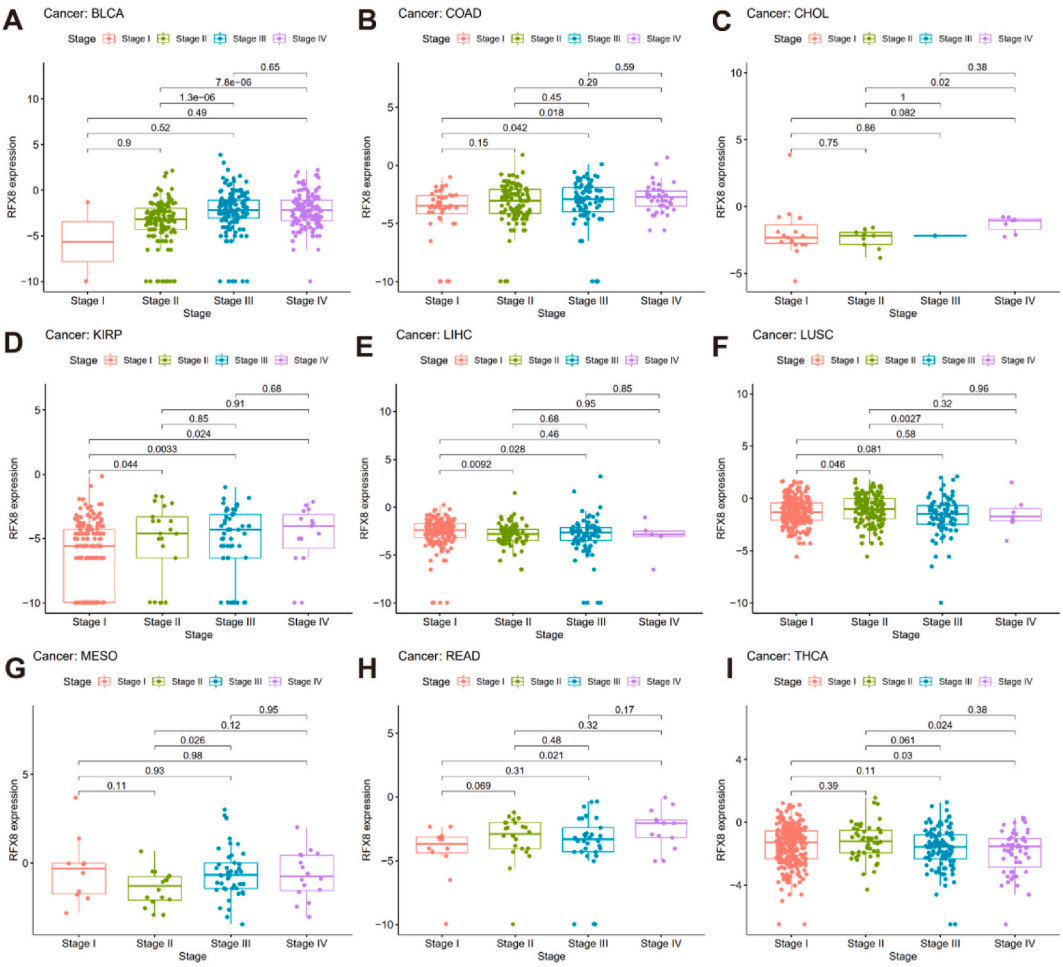

Fig. 5. Correlation analysis of RFX 8 expression and Four stages in BLCA **(A),** COAD **(B),** CHOL **(C),** KIRP **(D),** LIHC **(E),** LUSC **(F),** MESO **(G),** READ **(H)** and THCA **(I).**

poorer prognosis due to low lymphocyte and high M2 macrophage content [22]. The ESTIMATE, CIBERSORT, and checkpoint correlation analyses further elucidate the role of RFX8 in cancer immunity from a multidimensional pan-cancer perspective.

AML is the most common leukemia among the adult population. Motivated by the differential expression and stemness scores in AML, we explored RFX8's biological function in tumor cell lines. In vitro assays validated the tumor-promoting role of this gene. Moreover, a drug sensitivity analysis followed by in vitro validation was conducted. It is noteworthy that nelarabine, whose correlation coefficients ranked highest, was an orphan drug used for refractory T-cell acute lymphoblastic leukemia (T-ALL) until recently. It was repurposed to induce AML cell differentiation and death [47]. However, it failed to exhibit any effect in our cells. The heterogeneity of the genetic background in AML likely accounts for this discrepancy.

Chelerythrine, which ranked second highest, is a plant alkaloid with multiple bioactivities, including anticancer activity. Chelerythrine exerts mechanistic effects on PKC, MAPK, BCL2-related molecules, and MAPK, all of which control cell proliferation and death [48]. The application of chelerythrine has been hindered by its potential toxicity. Combination administration can alleviate both the dose and the toxicity of chelerythrine. According to our findings, the IC50 in U937 cells decreased from 20 μM to 5 μM following RFX8 knockdown, a relatively safe dose for normal cells [49]. These preliminary findings suggest that RFX8 can alter drug sensitivity and proliferation, making it an ideal treatment target alone or in combination. However, additional validation in an animal model and a search for downstream targets are needed.

In conclusion, our work focused on RFX-related genes from a pan-cancer perspective. We demonstrated their expression profiles and roles in immunity, stemness, and prognosis through bioinformatics analysis. A more specific study of RFX8 was conducted in silico and in vitro. Our work can facilitate future exploration of the molecular mechanisms and targeted therapies involving these genes.

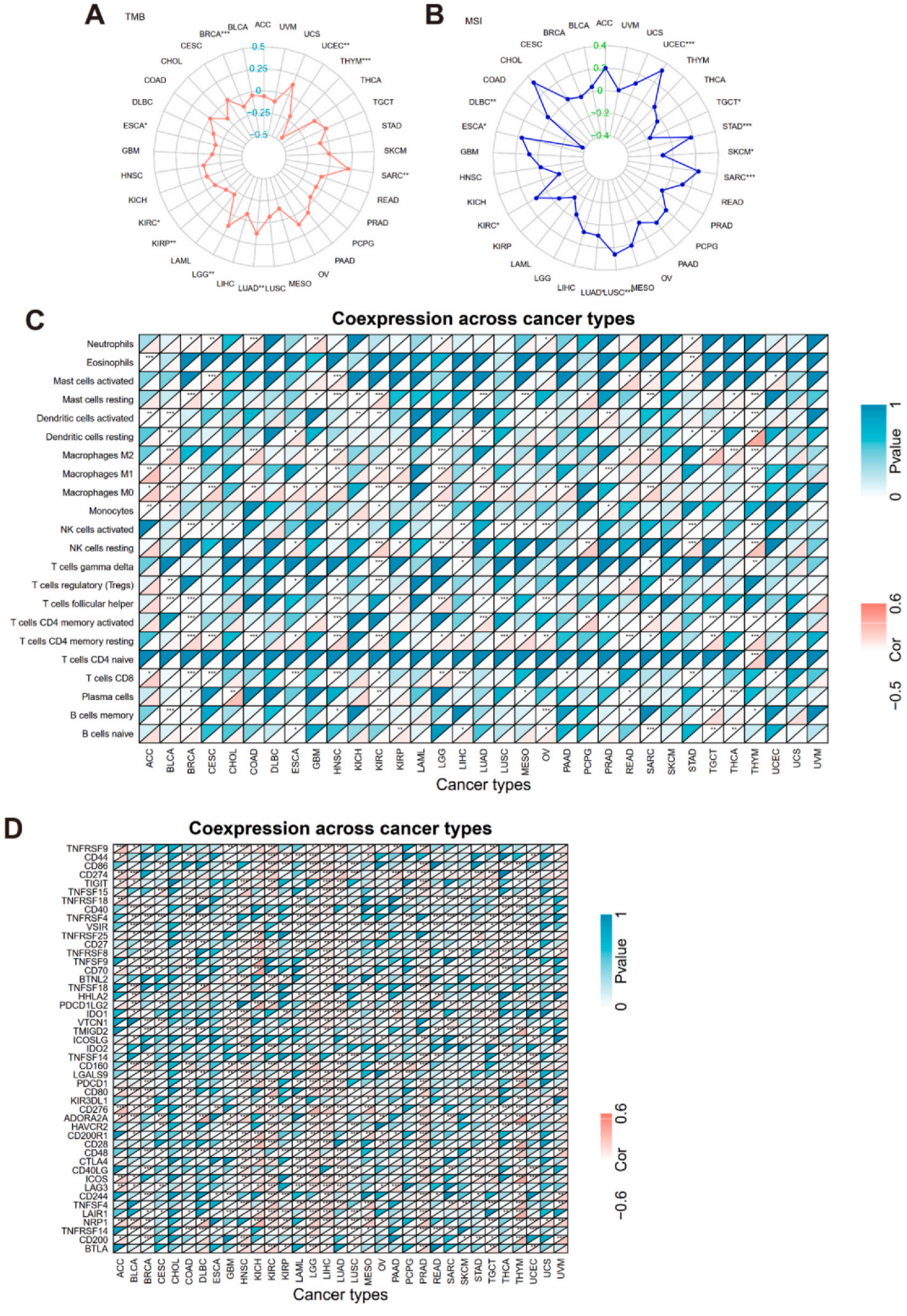

(caption on next page)

Fig. 6. Correlation of RFX 8 Gene Expression with Tumor Mutation Burden, Microsatellite Instability, Immune Cell Proportion, and Immune Checkpoint Gene Expression in Pan-Cancer. **(A and B)** RFX 8 gene expression correlation with TMB and MSI in 33 cancer types. The correlation coefficients are shown as points in the radar map. (**: $p < 0.01$; *: $p < 0.001$;: $p < 0.05$). **(C)** RFX 8 gene expression correlation with immune cell proportion in 33 cancer types. Positive and negative correlations are indicated by red and blue triangles. (***:$p < 0.001$; **:$p < 0.01$; *: $p < 0.05$). **(D)** RFX 8 gene expression correlation with 47 immune checkpoint gene expression in 33 cancer types. Positive and negative correlations are indicated by red and blue triangles. (***:$p < 0.001$; **:$p < 0.01$; *: $p < 0.05$). (For interpretation of the references to color in this figure legend, the reader is referred to the Web version of this article.)

Abbreviations

TF	Transcription factor
RFX	Regulatory Factor binding to the X-box, or Regulatory Factor X
RFXAP	Regulatory Factor X Associated Protein
RFXANK	Regulatory Factor X Associated Ankyrin Containing Protein
ACC	Adrenocortical Cancer
BLCA	Bladder Cancer
BRCA	Breast Cancer
CESC	Cervical Cancer
CHOL	Bile Duct Cancer
COAD	Colon Cancer
READ	Rectal Cancer
DLBC	Large B-cell Lymphoma
ESCA	Esophageal Cancer
FPPP	FFPE Pilot Phase II
GBM	Glioblastoma
LGG	Lower Grade Glioma
HNSC	Head and Neck Cancer
KICH	Kidney Chromophobe
KIRC	Kidney Clear Cell Carcinoma
KIRP	Kidney Papillary Cell Carcinoma
LAML	Acute Myeloid Leukemia
LGG	Lower Grade Glioma
LIHC	Liver Cancer
LUAD	Lung Adenocarcinoma
LUNG	Lung Cancer
LUSC	Lung Squamous Cell Carcinoma
MESO	Mesothelioma
OV	Ovarian Cancer
PAAD	Pancreatic Cancer
PANCAN	Pan-Cancer
PCPG	Pheochromocytoma & Paraganglioma
PRAD	Prostate Cancer
READ	Rectal Cancer
SARC	Sarcoma
SKCM	Melanoma
STAD	Stomach Cancer
TGCT	Testicular Cancer
THCA	Thyroid Cancer
THYM	Thymoma (THYM)
UCEC	Endometrioid Cancer
UCS	Uterine Carcinosarcoma
UVM	Ocular melanomas
TMB	tumor mutation burden
TME	tumor microenvironment
MSI	microsatellite instability
DNAss	DNA stemness score
RNAss	RNA stemness score
CHE	Chelerythrine
IC50	Half-maximal inhibitory concentration
DEG	Differential Expression Gene

Ethics approval and consent to participate

Sample collection and preparation have received informed consent from patients and have been approved by Qilu Hospital, Shandong University ethics committee. Ethical approval number: KYLL-2020(KS)-535.

Funding

This work was supported by the National Natural Science Foundation of China (Grant No: 82070164 and 82100186) and the

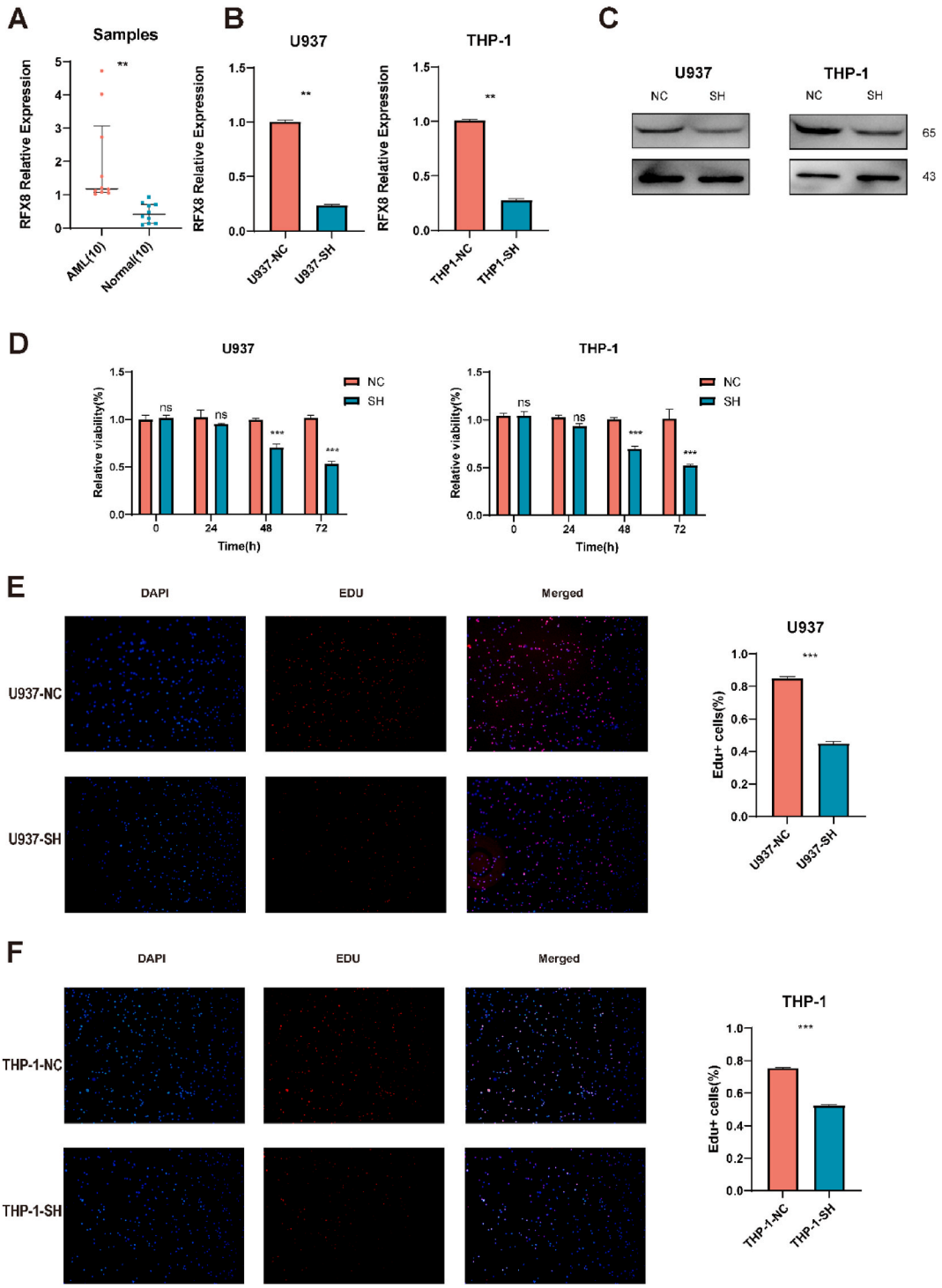

Fig. 7. Validation and Proliferation Analysis of RFX 8 Knockdown in AML Cell Lines. **(A)** RFX 8 mRNA expression in AML and normal samples. (***: $p < 0.001$; **:$p < 0.01$; *: $p < 0.05$). **(B and C)** RNA and protein knockdown efficiency of RFX 8 knockdown cell and control vector in U937 and THP-1 cell lines. (***:$p < 0.001$; **:$p < 0.01$; *: $p < 0.05$). (D) CCK8 assay of RFX 8 knockdown cell and control vector in U937 and THP1 cell lines. Viability values were calculated per 24h and final values at 72h were examined. (***:$p < 0.001$; **:$p < 0.01$; *: $p < 0.05$) **(E and F)** EdU assay of RFX 8 knockdown cell and control vector in U937 and THP-1 cell lines. Photos were taken at 72h shown as DAPI Edu and merged staining. Positive cell percentage (%) was qualified as in bar plot. (***:$p < 0.001$; **:$p < 0.01$; *: $p < 0.05$).

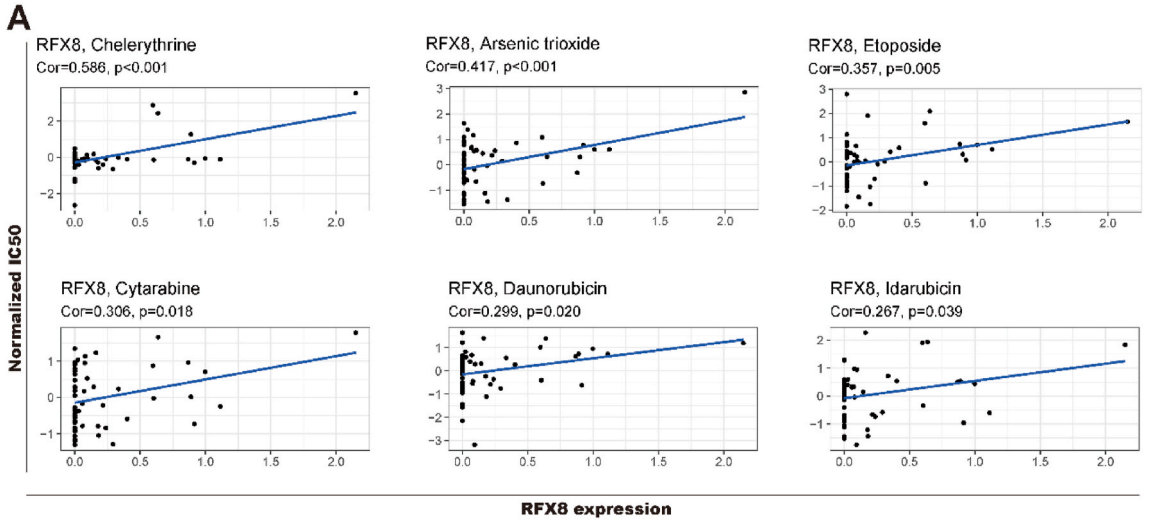

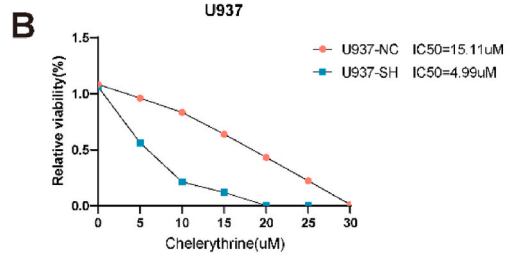

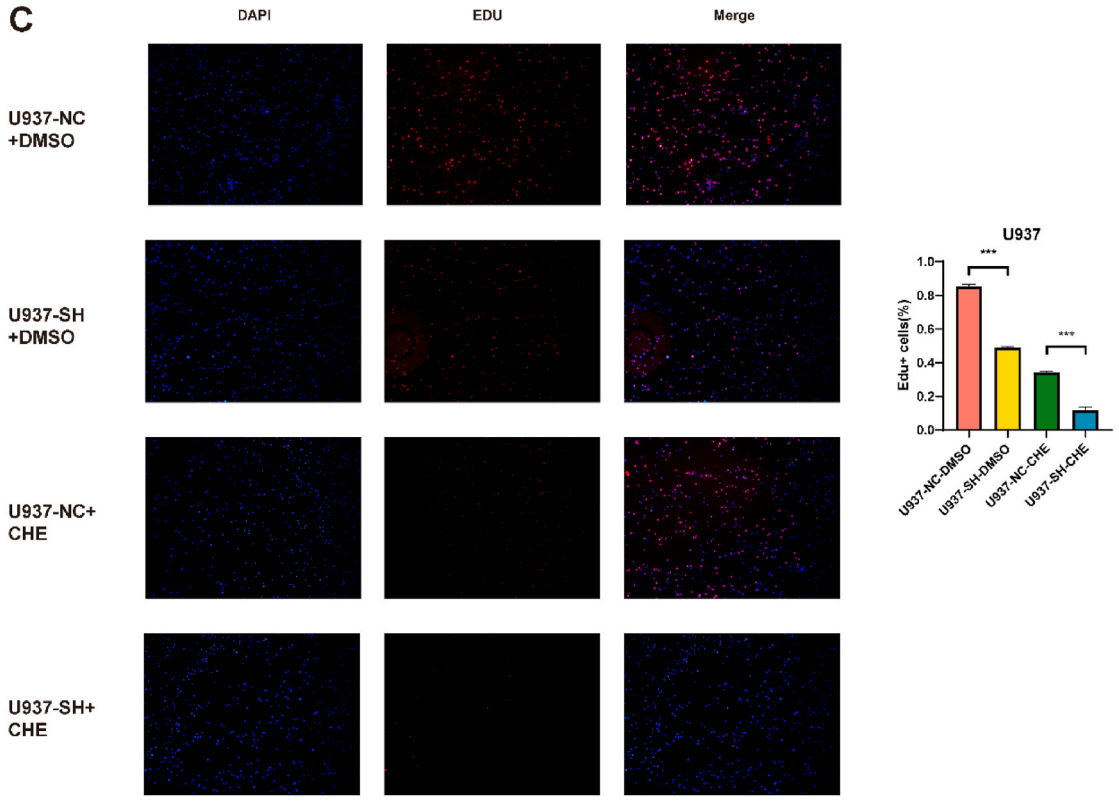

(caption on next page)

Fig. 8. Validation of RFX 8 as a Sensitizer to Chelerythrine (CHE). **(A)** Correlation analysis of RFX 8 expression and drug sensitivity. Each plot shows gene expression on the horizontal axis and IC50 value on the vertical axis. **(B)** CCK-8 assay of RFX 8 knockdown and control vector U937 cell line with varying concentrations of CHE. Viability values were calculated at 24h. **(C)** EdU assay of RFX 8 knockdown and CHE combination in U937 cell lines. Cells, with or without RFX 8 knockdown, were treated with 15 μM CHE or solvent DMSO for 72h. Positive cell percentage (%) is shown in the bar plot. (***:$p < 0.001$; **:$p < 0.01$; *: $p < 0.05$).

Natural Science Foundation of Shandong Province, China (Grant No: ZR2019PH073 and ZR2020QH093).

Data availability statement

All data generated or analyzed in this study can be acquired from the UCSC Xena(https://xenabrowser.net/datapages/), the GDC portal (https://portal.gdc.cancer.gov/), and the sources mentioned in Materials and Methods.

CRediT authorship contribution statement

Zelong Cui: Writing – original draft, Visualization, Methodology, Investigation, Formal analysis. **Yue Fu:** Methodology, Funding acquisition, Formal analysis. **Minran Zhou:** Methodology, Funding acquisition. **Huimin Feng:** Resources, Methodology, Investigation. **Lu Zhang:** Resources, Methodology. **Sai Ma:** Supervision, Resources, Methodology, Funding acquisition. **Chunyan Chen:** Writing – review & editing, Validation, Resources, Methodology, Investigation, Funding acquisition, Conceptualization.

Declaration of competing interest

The authors declare that they have no known competing financial interests or personal relationships that could have appeared to influence the work reported in this paper.

Appendix A. Supplementary data

Supplementary data to this article can be found online at https://doi.org/10.1016/j.heliyon.2024.e35368.

References

[1] K.S. Gajiwala, H. Chen, F. Cornille, B.P. Roques, W. Reith, B. Mach, et al., Structure of the winged-helix protein hRFX1 reveals a new mode of DNA binding, NATURE 403 (2000) 916–921.
[2] D. Sugiaman-Trapman, M. Vitezic, E.M. Jouhilahti, A. Mathelier, G. Lauter, S. Misra, et al., Characterization of the human RFX transcription factor family by regulatory and target gene analysis, BMC Genom. 19 (2018) 181.
[3] S. Lemeille, M. Paschaki, D. Baas, L. Morle, J.L. Duteyrat, A. Ait-Lounis, et al., Interplay of RFX transcription factors 1, 2 and 3 in motile ciliogenesis, Nucleic Acids Res. 48 (2020) 9019–9036.
[4] S.P. Choksi, G. Lauter, P. Swoboda, S. Roy, Switching on cilia: transcriptional networks regulating ciliogenesis, Development 141 (2014) 1427–1441.
[5] J. Piccand, P. Strasser, D.J. Hodson, A. Meunier, T. Ye, C. Keime, et al., Rfx6 maintains the functional identity of adult pancreatic beta cells, Cell Rep. 9 (2014) 2219–2232.
[6] W. Castro, S.T. Chelbi, C. Niogret, C. Ramon-Barros, S. Welten, K. Osterheld, et al., The transcription factor Rfx7 limits metabolism of NK cells and promotes their maintenance and immunity, Nat. Immunol. 19 (2018) 809–820.
[7] S. Hanna, A. Etzioni, MHC class I and II deficiencies, J ALLERGY CLIN IMMUN 134 (2014) 269–275.
[8] J.H. Bushweller, Targeting transcription factors in cancer - from undruggable to reality, Nat. Rev. Cancer 19 (2019) 611–624.
[9] J. Issac, P.S. Raveendran, A.V. Das, RFX1: a promising therapeutic arsenal against cancer, Cancer Cell Int. 21 (2021) 253.
[10] M. Taniwaki, Y. Daigo, N. Ishikawa, A. Takano, T. Tsunoda, W. Yasui, et al., Gene expression profiles of small-cell lung cancers: molecular signatures of lung cancer, Int. J. Oncol. 29 (2006) 567–575.
[11] D. Grisaru, J. Hauspy, M. Prasad, M. Albert, K.J. Murphy, A. Covens, et al., Microarray expression identification of differentially expressed genes in serous epithelial ovarian cancer compared with bulk normal ovarian tissue and ovarian surface scrapings, Oncol. Rep. 18 (2007) 1347–1356.
[12] Y. Qian, B. Cheng, J. Luo, Y. Hu, L. Gao, H. Cheng, CircRFX3 up-regulates its host gene RFX3 to facilitate tumorigenesis and progression of glioma, J. Mol. Neurosci. 72 (2022) 1195–1207.
[13] S. Legare, C. Chabot, M. Basik, SPEN, a new player in primary cilia formation and cell migration in breast cancer, Breast Cancer Res. 19 (2017) 104.
[14] H. Matsushita, A. Uenaka, T. Ono, K. Hasegawa, S. Sato, F. Koizumi, et al., Identification of glioma-specific RFX4-E and -F isoforms and humoral immune response in patients, Cancer Sci. 96 (2005) 801–809.
[15] D.B. Chen, X.W. Xie, Y.J. Zhao, X.Y. Wang, W.J. Liao, P. Chen, et al., RFX5 promotes the progression of hepatocellular carcinoma through transcriptional activation of KDM4A, SCI REP-UK 10 (2020) 14538.
[16] G. Ding, X. Xu, D. Li, Y. Chen, W. Wang, D. Ping, et al., Fisetin inhibits proliferation of pancreatic adenocarcinoma by inducing DNA damage via RFXAP/KDM4A-dependent histone H3K36 demethylation, Cell Death Dis. 11 (2020) 893.
[17] M. Song, M. Kuerban, L. Zhao, X. Peng, Y. Xu, Inhibition of RFX6 suppresses the invasive ability of tumor cells through the notch pathway and affects tumor immunity in hepatocellular carcinoma, Front. Oncol. 11 (2021) 801222.
[18] B.A. Fischer, S.T. Chelbi, G. Guarda, Regulatory factor X 7 and its potential link to lymphoid cancers, TRENDS CANCER 6 (2020) 6–9.
[19] L. Coronel, K. Riege, K. Schwab, S. Forste, D. Hackes, L. Semerau, et al., Transcription factor RFX7 governs a tumor suppressor network in response to p53 and stress, Nucleic Acids Res. 49 (2021) 7437–7456.
[20] B. Heuts, S. Arza-Apalategi, S. Frolich, S.M. Bergevoet, S.N. van den Oever, S.J. van Heeringen, et al., Identification of transcription factors dictating blood cell development using a bidirectional transcription network-based computational framework, SCI REP-UK 12 (2022) 18656.
[21] T. Liu, H. Gan, S. He, J. Deng, X. Hu, L. Li, et al., RNA helicase DDX24 stabilizes LAMB1 to promote hepatocellular carcinoma progression, Cancer Res. 82 (2022) 3074–3087.

[22] V. Thorsson, D.L. Gibbs, S.D. Brown, D. Wolf, D.S. Bortone, T.H. Ou Yang, et al., The immune landscape of cancer, Immunity 48 (2018) 812–830.
[23] K. Yoshihara, M. Shahmoradgoli, E. Martinez, R. Vegesna, H. Kim, W. Torres-Garcia, et al., Inferring tumour purity and stromal and immune cell admixture from expression data, Nat. Commun. 4 (2013) 2612.
[24] B. Chen, M.S. Khodadoust, C.L. Liu, A.M. Newman, A.A. Alizadeh, Profiling tumor infiltrating immune cells with CIBERSORT, Methods Mol. Biol. 1711 (2018) 243–259.
[25] Z. Wang, X. Guo, L. Gao, Y. Wang, Y. Guo, B. Xing, et al., Classification of pediatric gliomas based on immunological profiling: implications for immunotherapy strategies, MOL THER-ONCOLYTICS 20 (2021) 34–47.
[26] Z.J. Xu, X.L. Zhang, Y. Jin, S.S. Wang, Y. Gu, J.C. Ma, et al., Pan-cancer analysis reveals distinct clinical, genomic, and immunological features of the LILRB immune checkpoint family in acute myeloid leukemia, MOL THER-ONCOLYTICS 26 (2022) 88–104.
[27] T.M. Malta, A. Sokolov, A.J. Gentles, T. Burzykowski, L. Poisson, J.N. Weinstein, et al., Machine learning identifies stemness features associated with oncogenic dedifferentiation, CELL 173 (2018) 338–354.
[28] R. Bonneville, M.A. Krook, E.A. Kautto, J. Miya, M.R. Wing, H.Z. Chen, et al., Landscape of microsatellite instability across 39 cancer types, JCO PRECIS ONCOL 2017 (2017).
[29] D. Sha, Z. Jin, J. Budczies, K. Kluck, A. Stenzinger, F.A. Sinicrope, Tumor mutational burden as a predictive biomarker in solid tumors, Cancer Discov. 10 (2020) 1808–1825.
[30] K. Bialkowski, K.S. Kasprzak, A profile of 8-oxo-dGTPase activities in the NCI-60 human cancer panel: meta-analytic insight into the regulation and role of MTH1 (NUDT1) gene expression in carcinogenesis, FREE RADICAL BIO MED 148 (2020) 1–21.
[31] Z. Cui, Y. Fu, Z. Yang, Z. Gao, H. Feng, M. Zhou, et al., Comprehensive analysis of a ferroptosis pattern and associated prognostic signature in acute myeloid leukemia, Front. Pharmacol. 13 (2022) 866325.
[32] M. Palmeri, J. Mehnert, A.W. Silk, S.K. Jabbour, S. Ganesan, P. Popli, et al., Real-world application of tumor mutational burden-high (TMB-high) and microsatellite instability (MSI) confirms their utility as immunotherapy biomarkers, ESMO OPEN 7 (2022) 100336.
[33] S.S. Joshi, B.D. Badgwell, Current treatment and recent progress in gastric cancer, CA A Cancer J. Clin. 71 (2021) 264–279.
[34] E.R. Malone, M. Oliva, P. Sabatini, T.L. Stockley, L.L. Siu, Molecular profiling for precision cancer therapies, Genome Med. 12 (2020) 8.
[35] W. Jia, S. Liang, W. Lin, S. Li, J. Yuan, M. Jin, et al., Hypoxia-induced exosomes facilitate lung pre-metastatic niche formation in hepatocellular carcinoma through the miR-4508-RFX1-IL17A-p38 MAPK-NF-kappaB pathway, Int. J. Biol. Sci. 19 (2023) 4744–4762.
[36] J. Issac, P.S. Raveendran, M. Kunnummal, M. Angelin, S. Ravindran, B. Basu, et al., RXR agonist, Bexarotene, effectively reduces drug resistance via regulation of RFX1 in embryonic carcinoma cells, BBA-MOL CELL RES 1870 (2023) 119510.
[37] T. Ma, X. Zhou, H. Wei, S. Yan, Y. Hui, Y. Liu, et al., Long non-coding RNA SNHG17 upregulates RFX1 by sponging miR-3180-3p and promotes cellular function in hepatocellular carcinoma, Front. Genet. 11 (2020) 607636.
[38] Z. Zhang, Y. Chen, Y. Guo, H. Shen, J. Wang, H. Chen, RFX2 promotes tumor cell stemness through epigenetic regulation of PAF1 in spinal ependymoma, J. Neuro Oncol. 165 (2023) 487–497.
[39] Y. Yang, H. Li, Y. Liu, C. Chi, J. Ni, X. Lin, MiR-4319 hinders YAP expression to restrain non-small cell lung cancer growth through regulation of LIN28-mediated RFX5 stability, Biomed. Pharmacother. 115 (2019) 108956.
[40] T. Hou, L. Ye, S. Wu, Knockdown of LINC00504 inhibits the proliferation and invasion of breast cancer via the downregulation of miR-140-5p, OncoTargets Ther. 14 (2021) 3991–4003.
[41] Z. Qiu, C. Wang, P. Huang, Y. Yuan, Y. Shi, Z. Lin, et al., RFX6 facilitates aerobic glycolysis-mediated growth and metastasis of hepatocellular carcinoma through targeting PGAM1, Clin. Transl. Med. 13 (2023) e1511.
[42] N.M. Amankulor, Y. Kim, S. Arora, J. Kargl, F. Szulzewsky, M. Hanke, et al., Mutant IDH1 regulates the tumor-associated immune system in gliomas, Gene Dev. 31 (2017) 774–786.
[43] L. Spangenberg, P. Shigunov, A.P. Abud, A.R. Cofre, M.A. Stimamiglio, C. Kuligovski, et al., Polysome profiling shows extensive posttranscriptional regulation during human adipocyte stem cell differentiation into adipocytes, Stem Cell Res. 11 (2013) 902–912.
[44] J.C. Rausch, J.E. Lavine, N. Chalasani, X. Guo, S. Kwon, J.B. Schwimmer, et al., Genetic variants associated with obesity and insulin resistance in hispanic boys with nonalcoholic fatty liver disease, J. Pediatr. Gastroenterol. Nutr. 66 (2018) 789–796.
[45] E. Dalla, R. Picco, G. Novara, F.D. Moro, C. Brancolini, Identification of a gene signature for the prediction of recurrence and progression in non-muscle-invasive bladder cancer, Mol Biomed 3 (2022) 9.
[46] G. Sun, Y. Ge, Y. Zhang, L. Yan, X. Wu, W. Ouyang, et al., Transcription factors BARX1 and DLX4 contribute to progression of clear cell renal cell carcinoma via promoting proliferation and epithelial-mesenchymal transition, Front. Mol. Biosci. 8 (2021) 626328.
[47] H. Wang, X. He, F. Huang, H. Dong, W. Chen, Z. Li, et al., Repurposing nelarabine to induce differentiation of acute myeloid leukemia, Blood 136 (2020) 26.
[48] N. Chen, Y. Qi, X. Ma, X. Xiao, Q. Liu, T. Xia, et al., Rediscovery of traditional plant medicine: an underestimated anticancer drug of chelerythrine, Front. Pharmacol. 13 (2022) 906301.
[49] J. Ulrichova, Z. Dvorak, J. Vicar, J. Lata, J. Smrzova, A. Sedo, et al., Cytotoxicity of natural compounds in hepatocyte cell culture models. The case of quaternary benzo[c]phenanthridine alkaloids, TOXICOL LETT 125 (2001) 125–132.